Supplement of Atmos. Chem. Phys., 20, 13671–13686, 2020
https://doi.org/10.5194/acp-20-13671-2020-supplement

Atmospheric Chemistry and Physics
Open Access
EGU

Supplement of

From a polar to a marine environment: has the changing Arctic led to a shift in aerosol light scattering properties?

Dominic Heslin-Rees et al.

Correspondence to: Paul Zieger (paul.zieger@aces.su.se)

1 Data availability

Figure S1 shows the available data of nephelometer measurements used in this study.

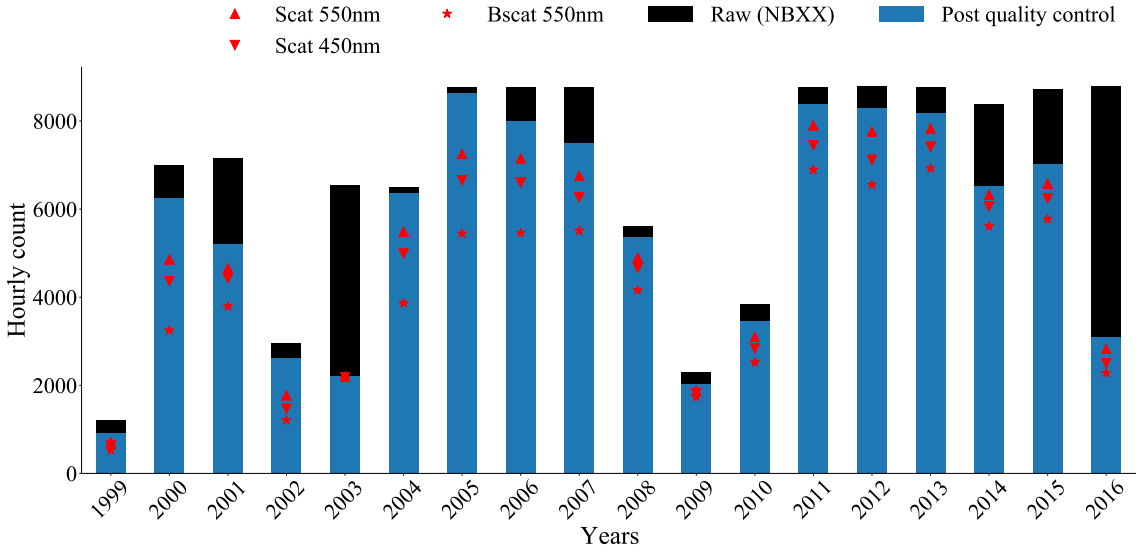

Figure S1. Data coverage: Black bars denote the number of hourly data points provided by the nephelometer before the quality control procedure. The blue bars denote the number of hourly data points used. Notice that the number of hourly data points for the light scattering coefficients ($\lambda = 450\,\text{nm}$ and $\lambda = 550\,\text{nm}$) and backscattering coefficient ($\lambda = 550\,\text{nm}$) are less than the blue bar. The bar blue represents the number of hourly averges of either one of these three main variables.

2 Particle light scattering coefficients compared to ambient relative humidity

Within this work, the effect of local cloud occurrence is explicitly addressed in the trend analysis. As a proxy for in-cloud data, the ambient relative humidity (RH) (see Fig. S2) is being used. Figure S2a shows that there is a slight influence from the ambient relative humidity on the RH at the sample outlet of the nephelometer. From Fig. S2b it is shown that increasing ambient RH results in increased σ_{sp} up to a point, after which the high levels of ambient RH associated with the presence of clouds begin to reduce the inlet collection efficiency. The point at which inlet efficiency is negatively impacted by the presence of clouds is approximately 95 %. The overall effect is deemed insignificant. Figure S2c shows that α declines with increasing ambient RH, suggesting that the aerosol particles take up water and thus increase in size despite the nephelometer measuring under dry conditions (i.e. sample outlet RH < 40%). After approximately 93% ambient RH, there is a slight upturn in α suggesting that the presence of clouds at the inlet acts to remove a proportion of larger particles. However, the median α for cloud-free conditions (i.e. < 95%) is larger suggesting in fact that the size distribution is shifted closer to the smaller particles; this observation is put down to the increasing uncertainties observed in the data.

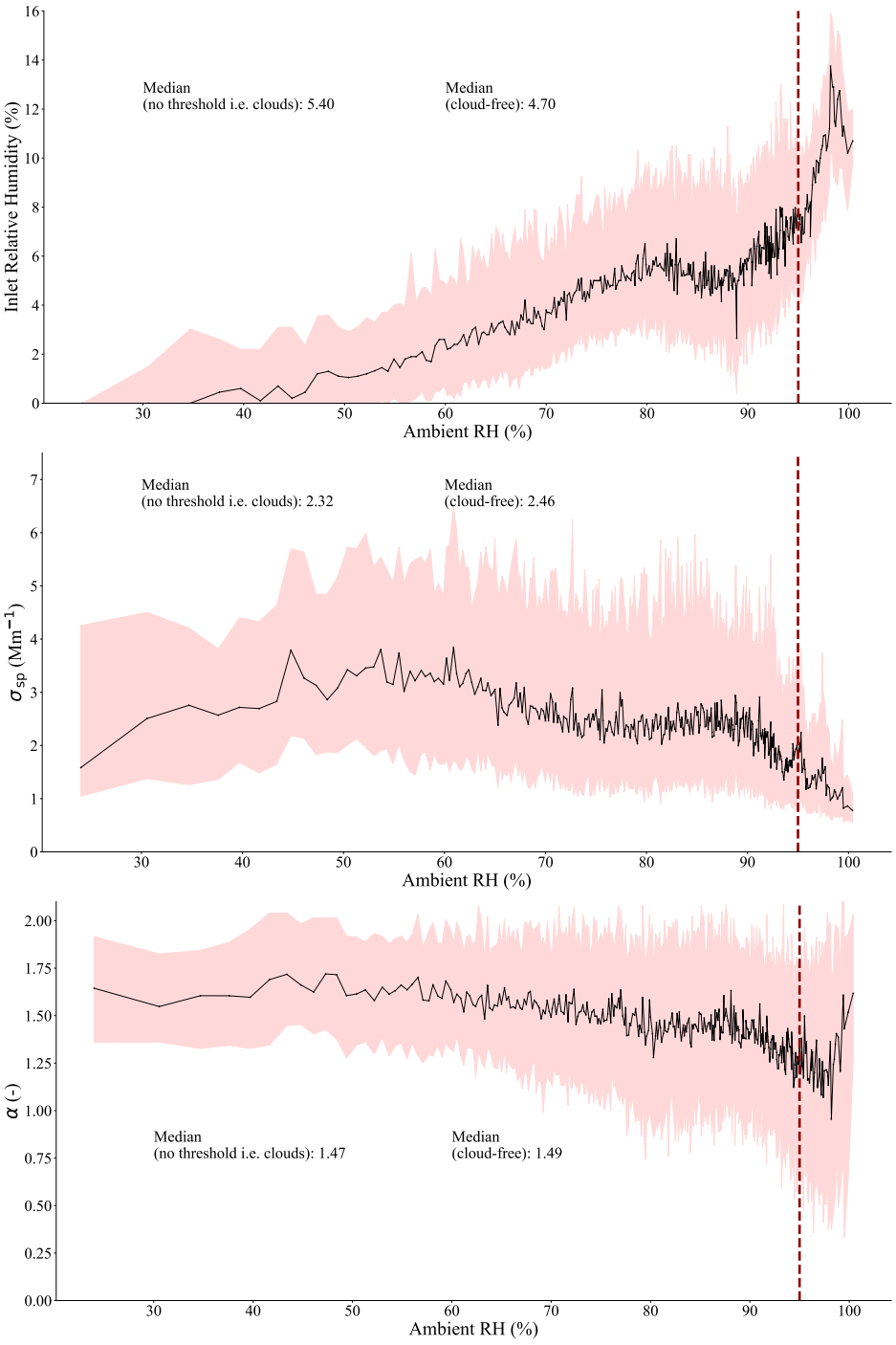

Figure S2. Effect of ambient relative humidity (RH): (a) The RH at the sample outlet vs. the ambient RH. (b) The scattering coefficient (σ_{sp}) vs. the ambient (RH). (c) The Ångström exponent (α) vs. the ambient (RH). The data is placed in bins of size 200 according to ascending values of ambient RH. The medians for each consecutive bin are calculated for the variables. The dotted red line (at ambient RH = 95%) displays the cut-off point, whereby in-cloud scavenging and inlet losses, influence σ_{sp} significantly.

3 Back trajectory calculations (method)

Figure S3 presents a detailed description of how the residence times over the three different surface types (land, ice and open water) are calculated. Note that the proportion of time the back trajectories spend above the mixed layer is also presented, and furthermore does not count towards the surface residence times.

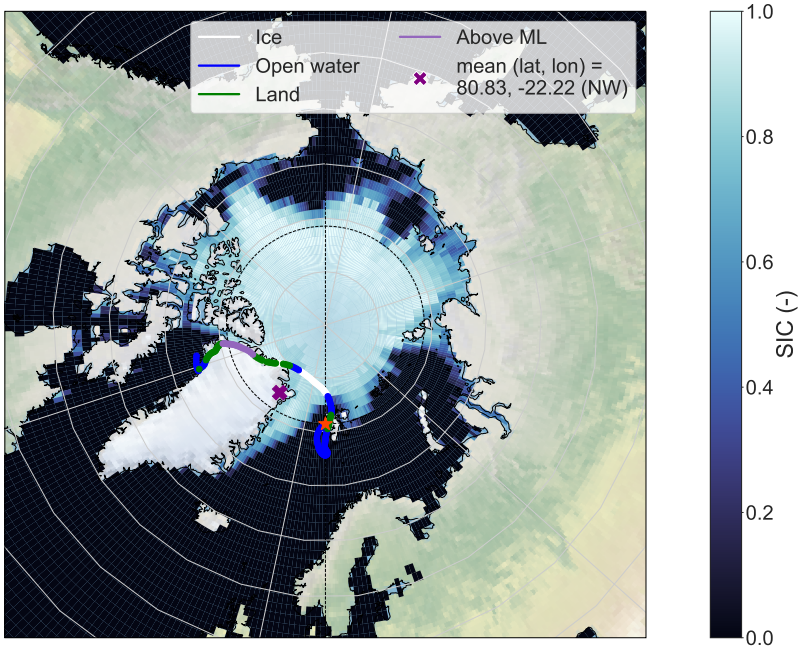

Figure S3. Example of the source attribution using back trajectory calculations: 168-h back trajectory arriving at the Zeppelin Observatory on 2008-10-05 at 13:00:00. Sections of the back trajectory are coloured as follows: above the mixed layer (purple), and within the mixed layer and above land (green), open water (blue), ice (white). The mean coordinates of the back trajectory, based only on the section that traverses through the ML, is denoted by the star. The red cross displays the location of the Zeppelin Observatory. The sea ice concentrations (SIC) at the time of arrival are displayed, based on monthly 1° x 1°-resolution satellite-derived Rayner et al. (2003) data. The meridian 11°89'E and parallel of 78°91'N lines are presented as black dashed lines for reference.

4 The contribution of coarse mode particles to particle light scattering

Coarse-mode particles contribute a significant proportion of the overall scattering observed at ZEP. To illustrate the importance of the coarse mode (here defined for particles above 1 μm), we have used particle size distribution measurements of fine and coarse mode from 2008 and Mie theory assuming dry spherical particles with a refractive index of $m = 1.51$ and a wavelength of $\lambda = 550$ nm (details on size distribution measurements and Mie code are given in Zieger et al., 2010). Figure S4 shows the mean monthly average of the particle surface size distribution and the differential scattering coefficient (the integral will deliver σ_{sp}) for July to October. As can be seen, in 2008 the coarse mode contributed on average between 20 and 45 % (at $\lambda = 550$ nm) to the particle light scattering and as such is an important contributor to overall light scattering properties. In Zieger et al. (2010), the coarse mode was identified as sea salt using chemical and trajectory analysis.

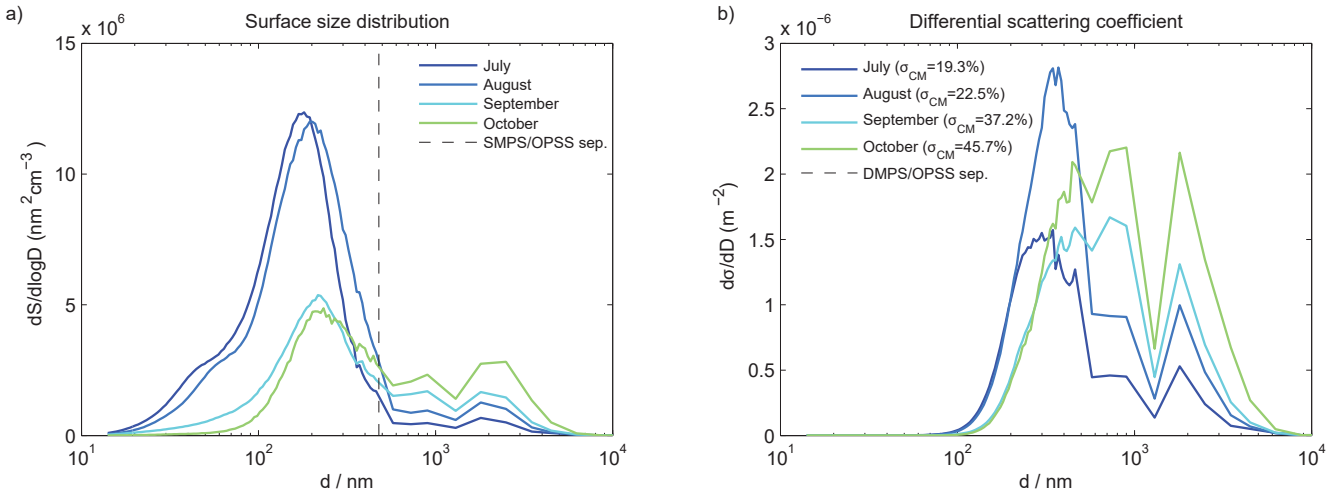

Figure S4. Monthly averages of (a) the particle surface size distribution and (b) the differential scattering coefficient (at $\lambda = 550$ nm) calculated using the SMPS (scanning mobility particle sizer) and OPSS (optical particle size spectrometer) measurements from Zieger et al. (2010). The percent contribution to light scattering of the coarse mode (CM) is given in the legend of panel b.

5 Results of trajectory analysis with a fixed sea ice

Figure S5 shows the relative surface contribution of the air masses arriving at ZEP. To investigate the effect of retreating Arctic sea ice on the surface type contributions alone, the contributions are calculated by holding the mean SIC at the annual cycle for 1999, The solid line denotes the surface type contributions based on the monthly sea ice concentrations (SIC). The dashed line is the SIC fixed to the values for the year of 1999. It can be seen that the relative contribution from different surface types does not change significantly between the dashed and solid lines. This suggests that the retreat in sea ice is not the main contributor to the increase in time spent by the back trajectories over the open water.

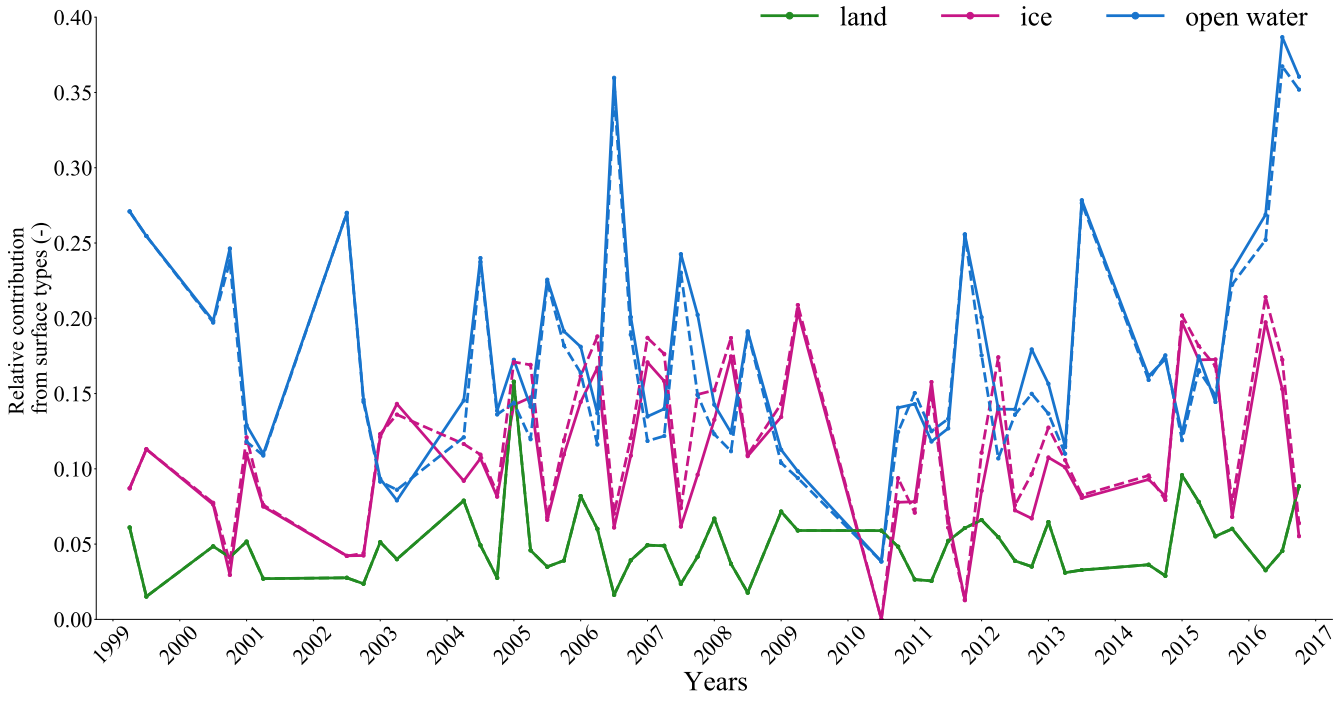

Figure S5. Relative surface contributions: the solid line represents the relative seasonal presence of each different surface type. The dashed line presents the same information but with sea ice concentrations set at 1999 values. Note the contributions do not include parts of the back trajectories above the mixed-layer (thus the sum is < 1).

6 Annual air mass contribution

The increased presence of south-west air masses in the summer is displayed in Fig. S6. The presence of SW air masses in the summer is consistent with previous studies (Freud et al., 2017; Osto et al., 2017). The dominant flow from the north during the winter and spring months is well documented by Stone et al. (2014).

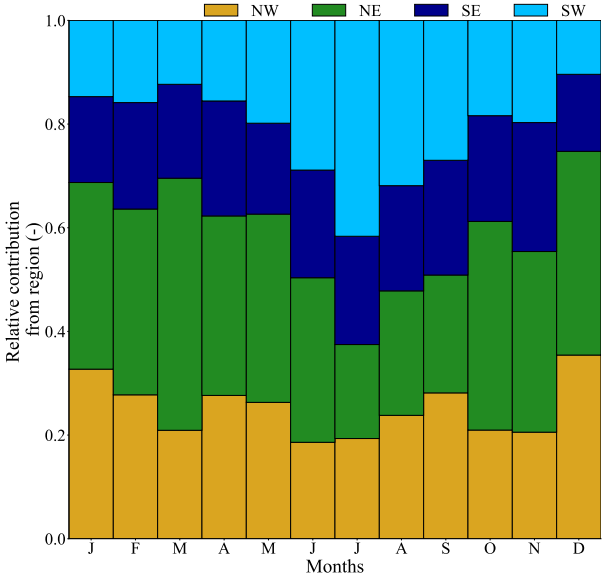

Figure S6. Annual variation of the monthly regional air mass contributions determined from the trajectory analysis for the entire observation period (1999-2016).

7 The annual contribution of the scattering Ångström exponent with respect to the main air mass sectors

In Figure S7, the hourly median α values are presented for each region, and for every year of observation, as a set of normalised histograms. The shift in air mass contributions is displayed in the relative histogram areas (A). The same years that feature peaks in their open water contributions (i.e. 2006, 2011, and 2016 in Fig S5) display decreases in their respective α medians. α for the western air masses are distinctly lower, compared to the eastern originated air masses. The western air masses are also more bimodal, suggesting the presence of more coarse-mode particles. It needs to be noted that the number of hourly data points for each season is not the same; spring and winter comprise of much more of the data (Tables S1 and S4) and thus annual medians are weighted more in their favour.

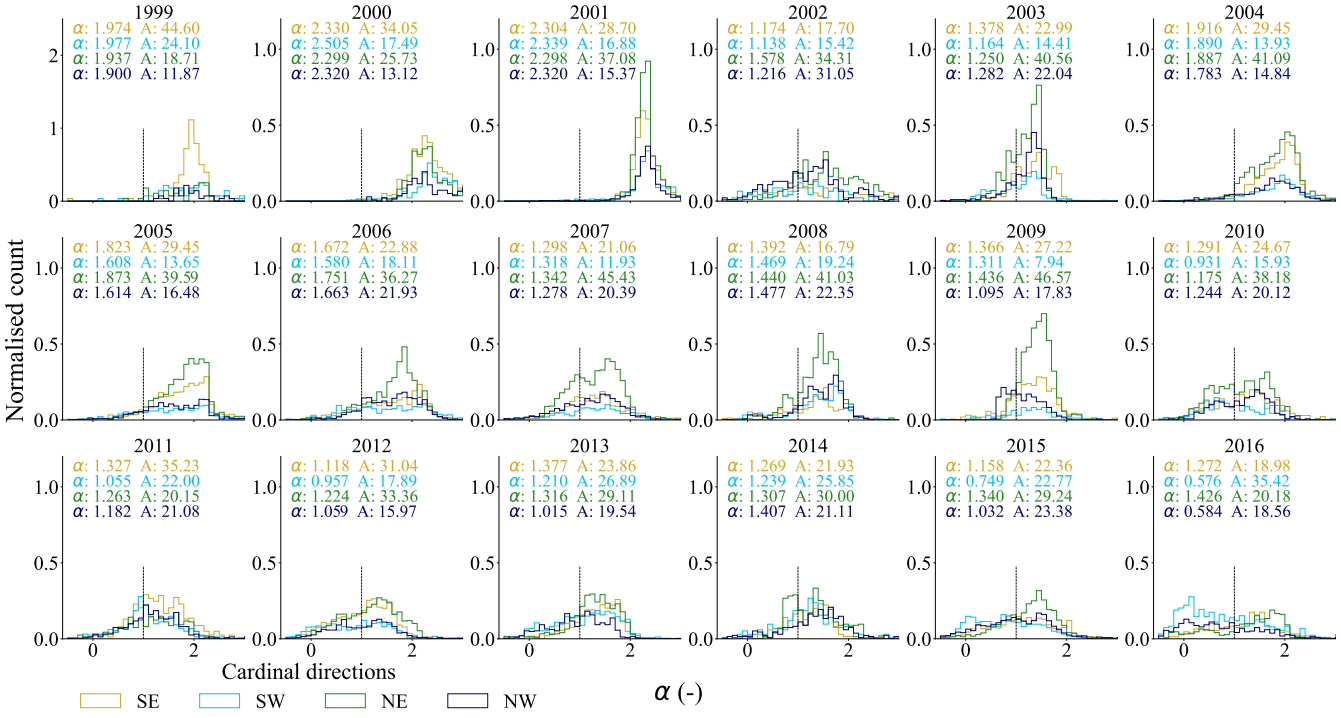

Figure S7. Annual histograms for hourly scattering Ångström exponent (α) medians of the four source regions namely, north-east (NE), south-east (SE), north-west (NW) and south-west (SW). The histograms are normalised by the total number of valid observations each respective year. The respective α medians for each region are given, along with the region's relative contribution (A (%)). The area left of the vertical dashed line, where ($\alpha < 1$), represents the approximate contribution from coarse-mode aerosol particles. Note the scale for the year 1999 is different.

8 Table of results

Tables S1, S2, S3 and S4 present the seasonal trends in the aerosol optical properties for both statistical tests (i.e. least mean square and seasonal Mann-Kendall test). The median for each season is also given, along with the number of hourly data points comprised of the points used in the trend analysis.

Table S1. Trends in scattering coefficient (σ_{sp}) for daily medians and seasonal medians: Theil-Sen slope estimator (TS) is presented as the change in Mm^{-1} per year and the relative change ($\%\ yr^{-1}$). Least mean square (LMS) is the percentage change based on a log transformation. For daily medians, the Man-Kendall test (MK test) is based on a "prewhitened" time series; total denotes the result of the seasonal MK test. Increasing (I) statistically significant trends are signified.

	Period	**Hourly points**	**Data points**	σ_{sp} **(Mm^{-1})**	**TS ($Mm^{-1}yr^{-1}$)**	**TS ($\%yr^{-1}$)**	**LMS ($\%yr^{-1}$)**	**MK**	**LMS**
Daily	spring	15760	827	3.34	0.05	1.37	1.75	I	I
	summer	7148	485	1.10	0.03	2.73	1.91	I	I
	autumn	10583	655	1.48	0.07	4.69	3.64	I	I
	winter	14042	720	3.02	0.19	6.18	6.46	I	I
	total	47533	2687	2.26	0.06	2.58	2.94	I	I
Seasonal	spring	15760	14	3.33	0.03	0.91	-0.26	-	-
	summer	7148	15	1.08	0.02	2.08	0.80	-	-
	autumn	10583	12	1.65	0.08	5.08	3.70	I	I
	winter	14042	11	3.24	0.21	6.49	4.72	I	I
	total	47533	52	2.09	0.05	2.28	1.29	I	-

Table S2. Trends in backscattering coefficient (σ_{bsp}) for daily medians and seasonal medians: Theil-Sen slope estimator (TS) is presented as the change in Mm^{-1} per year and the relative change ($\%\ yr^{-1}$). Least mean square (LMS) is the percentage change based on a log transformation. For daily medians, the Man-Kendall test (MK test) is based on a "prewhitened" time series; total denotes the result of the seasonal MK test. Increasing (I) statistically significant trends are signified.

	Period	**Hourly points**	**Data points**	σ_{bsp} **(Mm^{-1})**	**TS ($Mm^{-1}yr^{-1}$)**	**TS ($\%yr^{-1}$)**	**LMS ($\%yr^{-1}$)**	**MK**	**LMS**
Daily	spring	15476	826	0.44	0.01	1.42	0.37	I	-
	summer	6272	484	0.18	0.00	2.07	0.53	I	I
	autumn	9414	654	0.20	0.01	3.49	0.84	I	I
	winter	13365	721	0.38	0.02	5.31	1.87	I	I
	total	44527	2685	0.29	0.01	2.30	0.65	I	I
Seasonal	spring	15476	14	0.44	0.00	0.75	-0.02	-	-
	summer	6272	15	0.19	0.01	2.70	0.47	I	I
	autumn	9414	12	0.26	0.01	3.86	0.89	I	I
	winter	13365	11	0.42	0.03	6.12	1.47	I	-
	total	44527	52	0.29	0.01	2.49	0.44	I	-

Table S3. Trend in hemispheric backscattering fraction b (-) for daily medians and seasonal medians: Theil-Sen slope estimator (TS) is presented as the change per year and the relative change (% yr^{-1}). Least mean square (LMS) is the relative change based on a log transformation. For daily medians, the Man-Kendall test (MK test) is based on a "prewhitened" time series; all seasons denotes the result of the seasonal MK test. Decreasing (D) statistically significant trends are signified.

	Period	**Hourly points**	**Data points**	b **(-)**	**TS** ($\mathbf{yr^{-1}}$)	**TS** ($\%\mathbf{yr^{-1}}$)	**LMS** ($\%\mathbf{yr^{-1}}$)	**MK**	**LMS**
Daily	spring	15255	826	0.1295	0.0000	0.0088	-0.0160	-	-
	summer	5854	482	0.1493	-0.0008	-0.5398	-0.0830	D	D
	autumn	8842	644	0.1321	-0.0012	-0.9111	-0.1550	D	D
	winter	13077	720	0.1205	-0.0009	-0.7490	-0.1400	D	D
	total	43028	2672	0.1299	-0.0004	-0.3327	-0.0700	D	D
Seasonal	spring	15255	14	0.1275	0.0009	0.6859	0.0600	-	-
	summer	5854	15	0.1464	-0.0006	-0.4132	-0.0620	-	-
	autumn	8842	12	0.1304	-0.0013	-0.9852	-0.1050	-	-
	winter	13077	11	0.1195	-0.0001	-0.0711	-0.1110	-	-
	total	43028	52	0.1309	-0.0002	-0.1276	-0.0390	-	-

Table S4. Trend in scattering Ångström exponent (-) for daily medians and seasonal medians: Theil-Sen slope estimator (TS) is presented as the change per year and the relative change (% yr^{-1}). Least mean squares (LMS) is the percentage change based on a log transformation. For daily medians, the Man-Kendall test (MK test) is based on a "prewhitened" time series; all seasons denotes the result of the seasonal MK test. Decreasing (D) statistically significant trends are signified.

	Period	**Hourly points**	**Data points**	α **(-)**	**TS** ($\mathbf{yr^{-1}}$)	**TS** ($\%\mathbf{yr^{-1}}$)	**LMS** ($\%\mathbf{yr^{-1}}$)	**MK**	**LMS**
Daily	spring	15760	827	1.61	-0.06	-3.51	-5.01	D	D
	summer	7148	485	1.69	-0.07	-4.39	-4.93	D	D
	autumn	10583	655	1.20	-0.09	-7.17	-7.50	D	D
	winter	14042	720	1.31	-0.08	-5.85	-7.39	D	D
	total	47533	2687	1.46	-0.07	-4.91	-6.54	D	D
Seasonal	spring	15760	14	1.51	-0.05	-3.14	-1.59	D	D
	summer	7148	15	1.74	-0.07	-3.95	-2.55	D	D
	autumn	10583	12	1.20	-0.10	-8.68	-3.53	D	D
	winter	14042	11	1.22	-0.06	-4.83	-3.01	D	D
	total	47533	52	1.36	-0.07	-5.04	-2.65	D	D

References

Freud, E., Krejci, R., Tunved, P., Leaitch, R., Nguyen, Q. T., Massling, A., Skov, H., and Barrie, L.: Pan-Arctic aerosol number size distributions: seasonality and transport patterns, Atmos. Chem. Phys., 17, 8101–8128, https://doi.org/10.5194/acp-17-8101-2017, 2017.

Osto, M. D., Beddows, D., Tunved, P., Krejci, R., Stroem, J., Hansson, H.-C., Yoon, Y. J., Park, K., Becagli, S., Udisti, R., Onasch, T., Dowd, C. D. O., Simó, R., and Harrison, R.: Arctic sea ice melt leads to atmospheric new particle formation, Sci. Rep., 7, 3318, https://doi.org/10.1038/s41598-017-03328-1, 2017.

Rayner, N., Parker, D. E., Horton, E., Folland, C. K., Alexander, L. V., Rowell, D., Kent, E., and Kaplan, A.: Global analyses of sea surface temperature, sea ice, and night marine air temperature since the late nineteenth century, Journal of Geophysical Research: Atmospheres, 108, 2003.

Stone, R. S., Sharma, S., Herber, A., Eleftheriadis, K., and Nelson, D. W.: A characterization of Arctic aerosols on the basis of aerosol optical depth and black carbon measurements, Elem Sci Anth, 2, https://doi.org/10.12952/journal.elementa.000027, 2014.

Zieger, P., Fierz-Schmidhauser, R., Gysel, M., Ström, J., Henne, S., Yttri, K. E., Baltensperger, U., and Weingartner, E.: Effects of relative humidity on aerosol light scattering in the Arctic, Atmos. Chem. Phys., 10, 3875–3890, https://doi.org/https://doi.org/10.5194/acp-10-3875-2010, 2010.